Oscillation Characteristics of a High Power 300 GHz Band Pulsed Gyrotron for Use in Collective Thomson Scattering Diagnostics

Teruo SAITO, Shunsuke TANAKA, Ryuji SHINBAYASHI, Yoshinori TATEMATSU,
Yuusuke YAMAGUCHI, Masafumi FUKUNARI, Shin KUBO[1], Takashi SHIMOZUMA[1],
Kenji TANAKA[1] and Masaki NISHIURA[1]

Research Center for Development of Far-Infrared Region, University of Fukui, Fukui 910-8507, Japan
[1]*National Institute for Fusion Science, National Institute of Natural Sciences, Toki 509-5292, Japan*

A high power sub-THz pulsed gyrotron with a frequency of 303 GHz has been developed for use as the power source of the collective Thomson scattering (CTS) diagnostics in the Large Helical Device (LHD) at the National Institute for Fusion Science. Based on careful design considerations, a whispering gallery mode $TE_{22,2}$ was adopted to avoid mode competition. More than 320 kW was attained with single-mode oscillation. The spectrum of the oscillation frequency is very narrow and stable during the entire pulse duration for pulse widths up to 100 μs. No parasitic mode is excited at the turn-on and turn-off phases nor during the steady state of the oscillation pulse. In addition to the adoption of the whispering gallery mode, a fast but finite rise time of the beam voltage is an important role for the realization of single-mode oscillation. Self-consistent calculations show that, for the finite voltage rise time corresponding to the present experiment, gradual evolution to the high power regime is attained from backward wave oscillation. This high power regime corresponds to the hard self-excitation region in the case of instantaneous voltage rise.

1. Introduction

High frequency, high power gyrotrons are likely to suffer from mode competition; and hence the startup scenarios necessary to realize single-mode oscillation have been intensively studied [1–4]. Subsequently, gyrotrons at 170 GHz and 1 MW for use in the International Thermonuclear Experimental Reactor (ITER) have been successfully developed [5]. Now, higher frequency gyrotrons in the sub-THz band for DEMO are within the scope of development [6]. In addition, sub-THz gyrotrons are required as the power sources for the collective Thomson scattering (CTS) diagnostics. While CTS diagnostics using gyrotrons for electron heating around 100 GHz have already been developed [7–9], sub-THz waves are promising for CTS because they are almost free from refraction and absorption in plasmas and the background radiation stemming from strong electron cyclotron emissions (ECEs). We have developed a high power sub-THz pulsed gyrotron for improvement of the CTS diagnostics system in the large helical device (LHD) [10]. Use of a sub-THz gyrotron expands the CTS-applicable region of plasma parameters. In LHD, sub-THz CTS can be applied to the high density operation region, plasmas with impurity holes, etc.

Although the power level for CTS should be more than 100 kW to realize a sufficient signal-to-noise ratio [11],

pulse mode oscillation can be used. Pulsed gyrotrons with a low duty factor can be operated with a compact and simple power supply. In fact, we use a combination of a small capacitor bank and a semiconductor switch. This is advantageous for a diagnostic-use gyrotron. However, many pulses are generated in one plasma shot. Each pulse should consist of a single-mode oscillation during the entire pulse duration including the turn-on and turn-off phases because parasitic modes with frequencies outside of the stop band of a notch filter may destroy the very sensitive receiver system. Pulse mode operation was also adopted for CTS on LHD with a 77 GHz gyrotron to facilitate subtracting out the background radiation that originates from ECE. A sophisticated startup scenario for the gyrotron was necessary to suppress parasitic modes, and the oscillation condition was somewhat different from the highest power region [12]. Therefore, careful design consideration is very important to simultaneously realize single-mode oscillation and highest power operation with a simple power supply.

We first tried to develop a high power sub-THz gyrotron at the second harmonic resonance [13]. The magnetic field strength of a superconducting (SC) magnet can be reduced for second harmonic oscillations. However, a power level higher than 100 kW was not attainable owing to mode competition with a fundamental harmonic mode

_author's e-mail: saito_2729@fir.u-fukui.ac.jp_

[14, 15]. Alternatively, a fundamental harmonic gyrotron has been developed. Recent continuous wave (CW) 1 MW class gyrotrons for ITER [16] work in very high volume modes to reduce heat loss density on the cavity surface. However, for such modes, many competing modes are distributed near the working mode, and hence a sophisticated startup scenario is necessary [17]. On the other hand, the design concept of the present gyrotron relies on pulse mode operation because CW oscillation is not required in CTS diagnostics. Whispering gallery modes (WGMs) in a moderately oversized cavity are promising because the number of competing modes is reduced. WGMs are suitable to satisfy requirements for mode competition avoidance [18]. In fact, WGMs were used in the initial stage of the development of gyrotrons for fusion plasma heating; and stable oscillations without mode competition were verified [19, 20]. Therefore, WGMs are promising for complete suppression of spurious modes, even during the turn-on and turn-off phases of each oscillation pulse.

We first developed a prototype gyrotron with the $TE_{14,2}$ mode and used it to verify the design concept for stable single-mode oscillation [21]. Then, the same design concept was adopted for the practical gyrotron for use in CTS diagnostics in LHD. The oscillation mode is the $TE_{22,2}$ mode, which is a somewhat higher order mode than the $TE_{14,2}$ mode. The reason for the mode change is mainly to achieve the desired power levels with a duty cycle on the order of one percent. However, it should be noted that even WGMs are not free from mode competition. Mode competition calculations were carried out, and the $TE_{22,2}$ mode was adopted. The target power is 300 kW. The designed operating frequency is 303.3 GHz, which corresponds to a minimum in the frequency spectrum of ECE for the standard LHD operation. The cutoff density corresponding to 303 GHz is about 10^{21} m^{-3}. This gyrotron can be used in the high density operation mode of LHD.

Single-mode oscillation at the steady state is not sufficient. The absence of parasitic mode oscillations during the turn-on and turn-off phases was confirmed in the oscillation tests. The rise time of the beam voltage plays an important role. This point will be discussed later in the paper, based on self-consistent calculations that take into account the time variation of the axial field profile.

This paper includes the following four additional sections: Section 2 describes the design considerations. Section 3 shows the results of the oscillation test, and Sec. 4 is devoted to a discussion of single-mode oscillation. Finally, the present study is summarized in Sec. 5.

2. Design Considerations, Fabrication, and Testing of the 303 GHz Gyrotron

The sub-THz gyrotron for CTS is operated in a pulse mode. The design concept is the same as that of the pro-
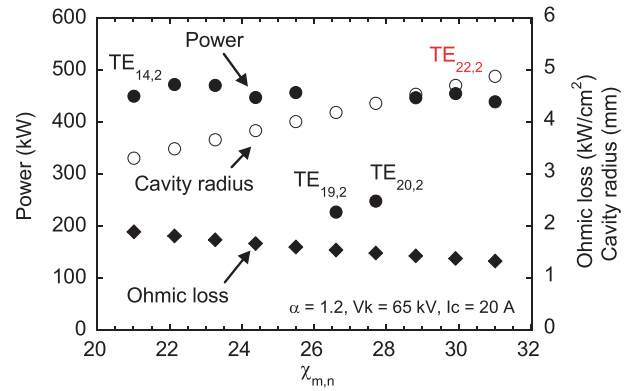

Fig. 1   Preliminary power calculation of candidate modes. The beam voltage and beam current are 65 kV and 20 A, respectively. Possible competing modes are included in the calculation. The cavity radius and the beam radius for each mode correspond to the oscillation frequency of 303.3 GHz.
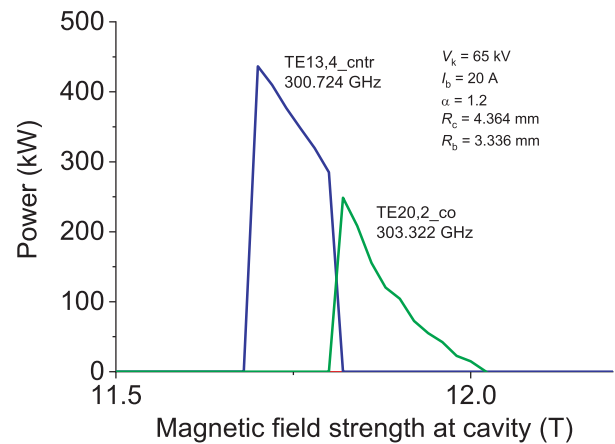

Fig. 2   Mode competition of the $TE_{20,2}$ co mode with the $TE_{13,4}$ counter mode. The beam voltage and beam current are 65 kV and 20 A, respectively. The beam radius corresponds to the maximum coupling radius for the $TE_{20,2}$ mode.

totype gyrotron [21]. A moderately over-moded cavity is used to satisfy simultaneous avoidance of mode competition and a low Ohmic loss on the cavity surface. Use of a WGM higher than that of the prototype gyrotron is necessary to extend the pulse width and increase the duty ratio up to 10%. Preliminary design consideration was carried out to find candidate modes. Figure 1 plots the stationary oscillation power obtained with a gyrotron design code [22] including competition with neighboring modes. This figure indicates that WGM modes are not always appropriate for high power oscillation. The $TE_{19,2}$ and $TE_{20,2}$ modes are subject to competition with neighboring modes. Figure 2 shows the mode competition between the $TE_{20,2}$ mode and the $TE_{13,4}$ mode. The $TE_{13,4}$ mode on the low frequency side suppresses the $TE_{20,2}$ mode in the region

of the magnetic field B at the cavity where the $TE_{20,2}$ mode should attain much higher power. The optimal beam radius for the $TE_{20,2}$ mode is assumed. Possible competing modes other than the $TE_{13,4}$ mode are also included in this calculation. The $TE_{13,4}$ mode is not very close to the $TE_{20,2}$ mode but eventually suppresses the $TE_{20,2}$ mode. Figure 1 also presents the average Ohmic loss on the cavity surface for an output power of 300 kW and a duty ratio of 10%. The calculation is based on Eq. (5.11) of Ref. [23]. The electric conductivity is assumed to be half of that of ideal copper at room temperature. In the case of $TE_{22,2}$ mode, the Ohmic loss on the cavity surface is lower than 2 kW/cm^2 by a safe margin.

The $TE_{22,2}$ mode was finally adopted. The same mode was also employed in [19, 20]. Oscillation characteristics of the $TE_{22,2}$ mode were examined in detail with the gyrotron design code, and stable single-mode oscillation was expected. An oscillation power higher than 300 kW was expected for a beam voltage V_k of 65 kV and a beam current I_B of 15 A with a velocity pitch factor α of 1.2 [24]. The cavity length was optimized to be 8 mm for this parameter set; moreover, even higher power levels can be expected for larger I_B. The design parameters are given in Ref. [24]. An electron gun of the triode type was specifically designed and optimized for the $TE_{22,2}$ mode, using the E-GUN code. The same design principle that was reported in Ref. [25] was used. The design predicted electron beams of high quality with the pitch factor α in the range

from 1.1 to 1.3 and sufficiently small velocity spreads up to I_B = 20 A [24].

Figure 3 is a photograph of the fabricated gyrotron. This gyrotron is to be mounted on a liquid He-free 12 T SC magnet. The diameter of the room temperature bore is 100 mm. An internal mode converter composed of a helical-cut Vlasov type launcher and four mirrors was installed into a rather narrow room [26]. The vacuum window was made of a c-axis cut crystal sapphire disk; its thickness was optimized for 303.3 GHz.

3. Oscillation Test

Oscillation tests have been carried out with a power supply composed of a 2 μF capacitor bank and a fast semiconductor switch (NISSIN PULSE ELECTRONICS CO., LTD., HVS-80KM10) [27]. Voltage regulation is not used. The value of V_k decreases during the pulse, but the decrement is negligible up to 100 μs (as shown later in Fig. 9). The voltage of the modulation anode U_{mod} was set with a simple resistive divider. Figure 4 presents the dependence of the oscillation intensity on B for V_k = 60 kV and I_B = 10 A. The output signal was measured with a pyroelectric detector placed in the beam radiating through the vacuum window. The $TE_{22,2}$ mode oscillation occurs in the region where B is greater than 11.6 T. The oscillation intensity has a maximum at B slightly higher than 11.6 T; it decreases abruptly for lower field strengths and decreases gradually for the higher fields. The small peak near 11.48 T corresponds to the $TE_{21,2}$ mode. Since the thickness of the vacuum window is optimized for the $TE_{22,2}$ mode, the amplitude of the $TE_{21,2}$ mode is very weak owing to the large reflection off the vacuum window. Strong oscillation of the $TE_{21,2}$ mode can be obtained with a double disk configuration [28]. Details of the double disk effect will be published elsewhere.

The output power P was measured with a water load. Figure 5 shows P as a function of I_B for V_k of 60 kV and

Fig. 3 Photograph of the 303 GHz gyrotron. A Gaussian-like beam is radiated through the vacuum window located at the left hand side.
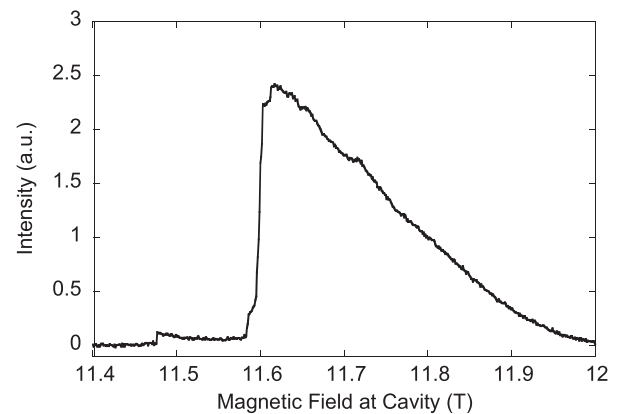

Fig. 4 Magnetic field dependence of the oscillation intensity of the $TE_{22,2}$ mode for a beam voltage and beam current of 60 kV and 10 A, respectively.

65 kV. The magnetic fields at which P was measured correspond to the B region where the oscillation intensity is a maximum as shown in Fig. 4. Other parameters such as U_{mod} and the auxiliary coil current to adjust the beam radius were optimized for each data point. A maximum power higher than 320 kW for $V_k = 65$ kV and $I_B = 15$ A was obtained [29]. The oscillation efficiency was higher than 30%. The experimental results are essentially consistent with the calculations, with α ranging from 1.1 to 1.3.

The radiation pattern was measured by using an infrared camera to record the temperature profile on a polyvinyl chloride plate located in front of the vacuum window. Figure 6 shows the radiation pattern at a distance of 1000 mm from the flange of the vacuum window. A Gaussian-like radiation pattern was obtained although a small fraction of higher order modes was observed [24]. The width along the vertical direction was smaller than that expected from the mode converter design calculations by about 15% and the radiation pattern was somewhat elliptic. The radiation beam can be tailored to an axi-symmetric Gaussian beam with an external matching optics unit designed based on the measured patters [30].
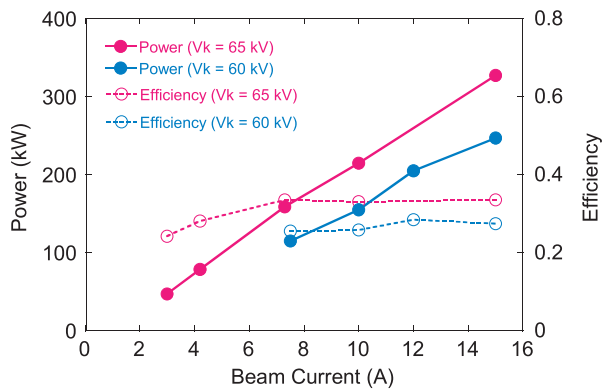
Measurement of the oscillation frequency using a Fabry-Perot interferometer verified single-mode oscillation of the $TE_{22,2}$ mode [24]. A more precise frequency measurement was carried out with a heterodyne receiver system. The measured frequency was 303.26 GHz when $V_k = 65$ kV, $I_B = 15$ A, and $B = 11.67$ T. This frequency is very close to the designed $TE_{22,2}$ mode frequency. The cavity was fabricated so that its diameter was maintained to within an accuracy of 1 μm. Figure 7 presents a typical frequency spectrum measured with a heterodyne receiver system. The spectrum is very narrow, and the full 3 dB width is smaller than 10 MHz. Parasitic modes were searched for over a wide frequency band, ranging from 290 GHz to 312 GHz, using the same heterodyne receiver system. No oscillation other than the $TE_{22,2}$ mode was observed throughout the duration of the pulse, including the turn-on and the turn-off phases. The dynamic range of this measurement was about 40 dB. This is larger than the power

Fig. 5   Power and the efficiency are plotted as functions of the beam current for the beam voltages of 60 kV and 65 kV.

Fig. 7   Frequency spectrum of the $TE_{22,2}$ mode. The beam voltage and the beam current are 65 kV and 15 A, respectively. The small peak on the lower frequency side is a marker indicating the center frequency stemming from frequency analysis in a fast digital oscilloscope.
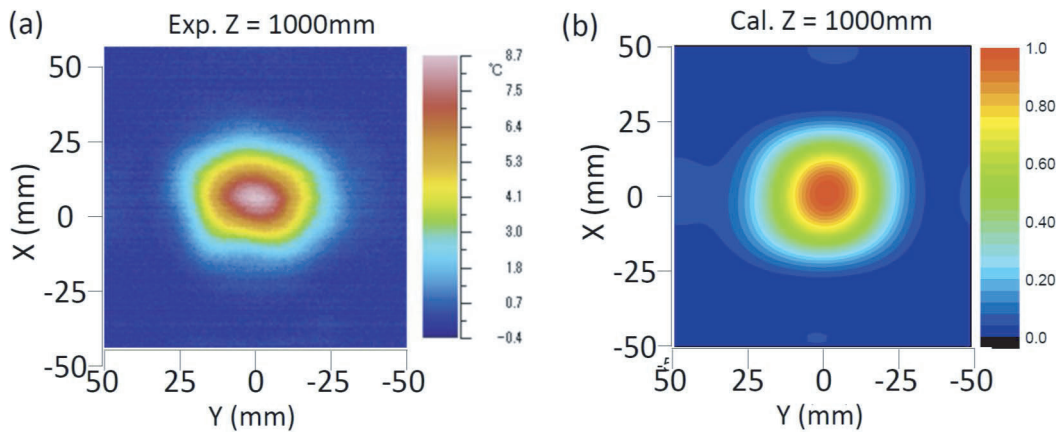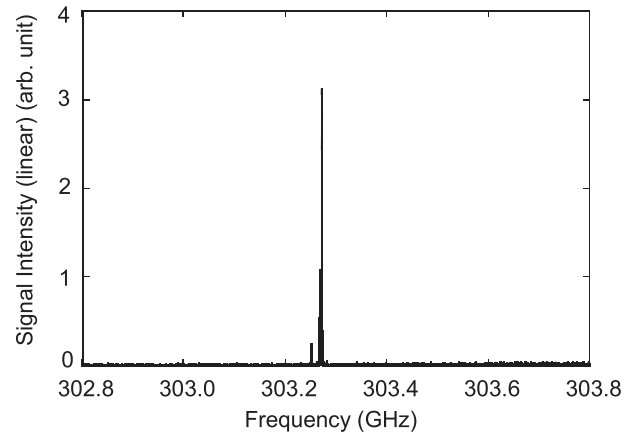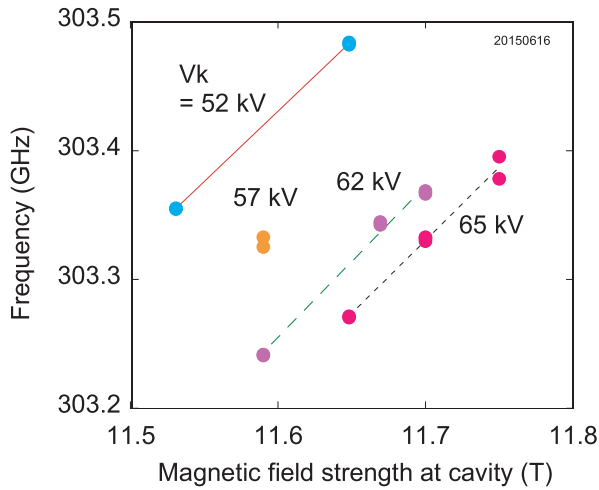

Fig. 6   (a) Radiation pattern of the gyrotron measured as a thermal image on an absorber plate and (b) calculated radiation pattern. The Y and X axes correspond to the horizontal and vertical directions in the experimental room, respectively.

Fig. 8　Frequency variation as a function of the magnetic field strength B at the cavity for various beam voltages. The beam current ranges from 11 A to 13 A.
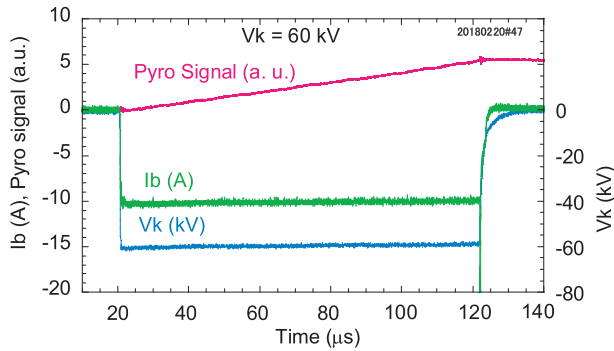

Fig. 9　Waveforms of a 100 μs oscillation. The beam voltage and beam current were set at 60 kV and 10 A, respectively.

Fig. 10　Time variation of the oscillation frequency. The beam voltage and beam current were set at 60 kV and 10 A, respectively.

range expected for the spectrum of the scattered wave [10]. Single-mode steady state oscillation of the $TE_{22,2}$ mode was attained at the value of B where the maximum power of the $TE_{22,2}$ mode was obtained with a simple power supply. A sophisticated startup scenario was not necessary.

A notch filter is used in CTS experiments to protect the highly sensitive receiver system from energy at the gyrotron frequency that stems from scattering off the vacuum vessel. The center frequency of the notch filter is 303.3 GHz and the full notch width is 0.5 GHz. The oscillation frequency varies slightly with the operation parameters such as V_k and B. Therefore, frequency control within the notch width is very important for application to CTS. Figure 8 indicates controllability of the frequency. The frequency variation with B and V_k is less than ±150 MHz, which is smaller than the notch width by a safe margin.

The pulse width was 5 to 10 μs in the oscillation tests describe above. Then, the pulse width was extended up to 100 μs. Relevant waveforms are plotted in Fig. 9. The beam voltage decreases slightly during the pulse because
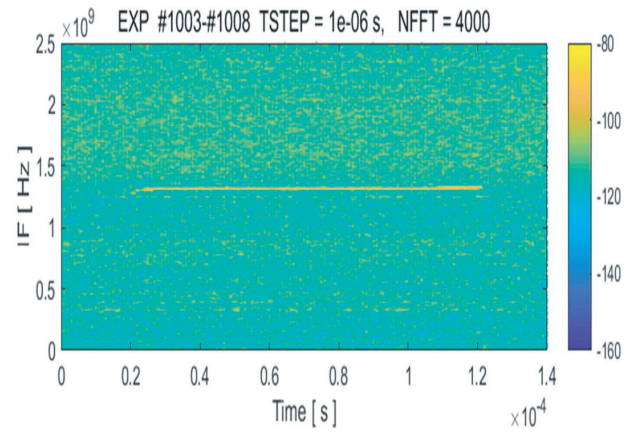
voltage regulation is not employed in the power supply. The oscillation signal was measured using a pyroelectric detector in the time integration mode. The linear increase in this signal indicates very stable power throughout the entire duration of the 100 μs pulse. This pulse width is sufficient for use in CTS diagnostics. The gyrotron will be operated with a pulse repetition rate of several tens of Hz in the CTS experiments. Figure 10 indicates the time variation of the frequency spectrum for the same pulse as shown in Fig. 9. The intermediate frequency about 1.3 GHz corresponds to a gyrotron frequency of 303.3 GHz. Figure 10 shows that the oscillation frequency is very stable during the entire pulse, and the frequency variation is less than 15 MHz. This is much smaller than the frequency width of the scattered wave [10].

The oscillation frequency f may change owing to expansion of the cavity radius a due to the Ohmic loss on the cavity surface during several-second plasma shot of LHD. Although f depends on the operation conditions, it is basically determined by a as long as B and V_k are fixed, and its change Δf depends on the variation of the cavity radius Δa as $\Delta f/f \approx -\Delta a/a$. We can estimate $\Delta f/f$ based on the measurements for a 77 GHz gyrotron [31] and a 140 GHz gyrotron [32]. Oscillation powers around 500 kW were somewhat higher than 300 kW of the present gyrotron. Both measurements indicated $\Delta a/a \approx 1.3 \times 10^{-4}$ for the initial 10 ms and $\approx 4 \times 10^{-4}$ or lower for 40 ms. Four second oscillation of the present 303 GHz gyrotron with a pulse width of 100 μs and a repetition rate of 10 Hz is equivalent to 40 ms because the Ohmic loss on the cavity surface is designed for the duty ratio of 10%. A cavity expansion of $\Delta a/a \approx 4 \times 10^{-4}$ leads to a decrease in f about 120 MHz. This is lower than the half width 250 MHz of the stop band of the notch filter by a factor of two. For a longer plasma shot or a higher repetition rate, setting at a higher initial oscillation frequency will be effective (see Fig. 8).

4. Discussion

Single-mode oscillation of the TE$_{22,2}$ mode was verified experimentally. The use of a WGM is one of the reasons why we were able to achieve oscillation free from parasitic modes without having to resort to sophisticated voltage control of the modulation anode. In addition to this, the very fast—but finite—rise time of the beam voltage also plays an important role. The beam voltage reaches 65 kV in about 0.25 µs (about 0.25 kV/ns) in the present experiment. A fast semiconductor switch enables this short rise time [27]. Suppression of parasitic modes for a voltage rise time shorter than 1 µs was predicted [33]. A theoretical study with a finite voltage rise time corresponding to the present gyrotron has also predicted single-mode oscillation of the TE$_{22,2}$ mode [34]. Here, we discuss the effect of the voltage rise time in more detail.

The beam voltage increases during the turn-on phase of each pulse. Hence, the relativistic electron cyclotron frequency ω_c varies with time; and consequently, the detuning factor $\Delta = 2(1 - \omega_c/\omega)/\beta_\perp^2$ also varies with time. Here ω is the oscillation frequency, $\beta_\perp = v_\perp/c$ with the electron velocity $v_\perp$ perpendicular to the magnetic field line, and c is the velocity of light. The relevant quantities are evaluated at the cavity entrance. The oscillation characteristics strongly depend on Δ, and the maximum power of a gyrotron is usually realized for Δ around $0.5 \sim 0.7$ [35]. However, this region exists in the hard self-excitation region [36]. Since ω is roughly equal to the resonance frequency of the cavity, Δ depends on V_k and B. A self-consistent analysis with a non-stationary axial field structure predicts the start of oscillation with a backward wave mode with a negative Δ and a gradual transition to the high power gyrotron mode while retaining the same transverse mode [33]. For the present gyrotron, Δ of the TE$_{22,2}$ mode is slightly negative at the time when the pulse starts, even when B is set close to the value that corresponds to the maximum steady-state output power. The single-mode oscillation observed in the present gyrotron presents a good case study of the theoretical prediction.

The time evolution of the TE$_{22,2}$ mode is calculated with the self-consistent gyrotron code including mode competition [22]. The cavity decay time $\tau_d = Q/\omega$ is about 1 ns for the present gyrotron with the cavity Q around 2000 and ω around $2\pi \times 300$ GHz. The electron transit time $\tau_p = L/c\beta_\parallel$ through the cavity length L is shorter than 0.1 ns when the normalized parallel velocity $\beta_\parallel$ is around 0.3, which corresponds to the present operation condition. Therefore, each electron passing through the cavity sees a quasi-stationary wave field. The normalized cavity length μ is about 11, and the normalized beam current I_0 is about 0.05 for the standard definition of μ and I_0 [35]. These parameters in fact correspond to hard self-excitation.

Figure 11 presents the calculated time evolution. The beam voltage increases to the steady state value of 65 kV with the experimental rate of 0.25 kV/ns, but starts from 40 kV to save calculation time. The starting voltage does not affect the situation. Since the beam current increases very rapidly under the temperature-limited-mode operation of the electron gun, the value of I_B is fixed at 15 A. The modulation anode voltage U_{mod} varies proportionally to V_k corresponding to the resistive divider of the power
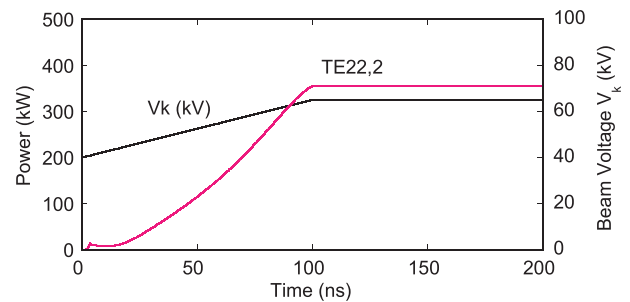

Fig. 11   Time evolution calculation with the mode competition code. The beam voltage has a finite voltage rise time. The beam voltage, beam current, and velocity pitch factor at the steady state are 65 kV, 15 A, and 1.2, respectively. The magnetic field at the cavity is 11.70 T.
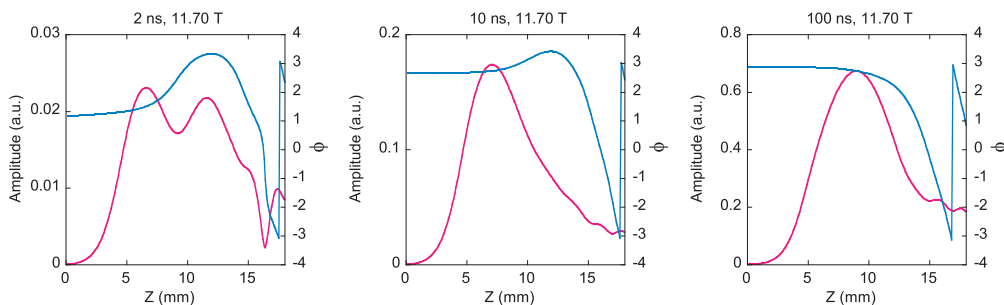

Fig. 12 Time evolution of the axial profiles of the field amplitude and the phase in the cavity are shown. The red lines represent the axial field profiles and the blue lines stand for the phase in radian. Parameters correspond to those in Fig. 11. The three panels represent three specific times: 2 ns, 10 ns and 100 ns, respectively. The detunig factors are −0.03, 0.1 and 0.67, respectively. The constant radius section of the cavity is from 5 mm to 13 mm. Down taper and up taper are attached to the left hand side and the right hand side.

supply used in the present experiment. The ratio of U_{mod} to V_k is 0.536. The value of α also varies with V_k and U_{mod}. The time variation of α is calculated with the relativistic adiabatic conservation law of the magnetic moment of electrons to simplify the calculation. Its steady state value of 1.2 is determined based on the design calculation of the electron gun. The magnetic field strength B of 11.70 T corresponds to the maximum steady state power of the $TE_{22,2}$ mode for $V_k = 65$ kV. The region of B slightly lower than 11.70 T is the oscillation region of the $TE_{21,2}$ mode. The beam radius is set at the optimum value for the $TE_{22,2}$ mode.

The $TE_{22,2}$ mode starts to grow with V_k and attains a steady state power. The $TE_{21,2}$ mode and other possible competing modes between the $TE_{22,2}$ mode and the $TE_{21,2}$ mode are included in the calculation. No mode other than the $TE_{22,2}$ mode oscillates during the turn-on phase and the steady state. In other words, the $TE_{22,2}$ mode pulls itself up to the highest power state.

Figure 12 presents the axial field profiles for three cases with different values of Δ: -0.03, 0.1, and 0.67. The phase profile indicates that oscillation starts from a backward wave with a slightly negative value of Δ. Transition from the backward wave to a forward wave takes
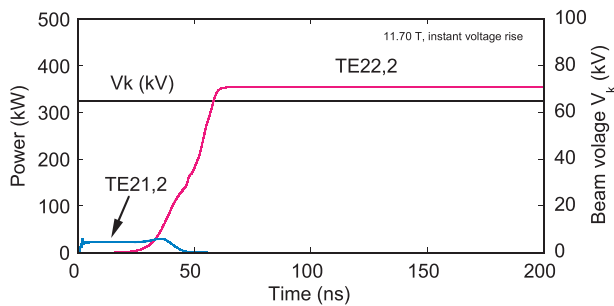

Fig. 13 Time evolution calculation with the mode competition code. The beam voltage rises instantaneously. The beam voltage and beam current at the steady state are 65 kV and 15 A, respectively.
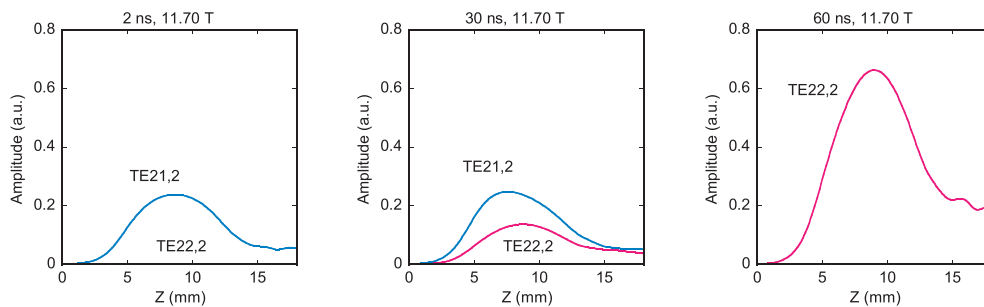
place with increasing Δ. Finally, gyrotron oscillation with a standing wave with a slightly forward wave feature near the cavity exit is established. Even though it is impossible for oscillation to start when the value of Δ is large, the high frequency field can grow from a low amplitude backward wave with a slightly negative Δ.

The situation changes for an instantaneous voltage rise. Figure 13 plots time evolution for the same set of relevant modes. The beam voltage, the modulation anode voltage, and the velocity pitch factor are constant and equal to those at the steady state in Fig. 11. The detuning factors of the $TE_{21,2}$ mode and the $TE_{22,2}$ mode are 0.08 and 0.67, respectively. The beam radius is set at the optimum value for the $TE_{22,2}$ mode. The $TE_{21,2}$ mode with the optimum beam radius nearly equal to that of the $TE_{22,2}$ mode starts to oscillate first, and then the $TE_{22,2}$ mode starts to grow in turn. The steady state powers in Figs. 11 and 13 are almost equal. The $TE_{22,2}$ mode does not grow when the $TE_{21,2}$ mode is not included in the calculation. This is a typical case of hard self-excitation [36]. Figure 14 shows the axial field profiles at three different times. The $TE_{21,2}$ mode exists in the soft self-excitation region and can start up itself. It generates phase bunching suitable for the $TE_{22,2}$ mode. Then, the $TE_{22,2}$ mode starts to grow with assistance of the $TE_{21,2}$ mode and finally suppresses the $TE_{21,2}$ mode. The remarkable difference between this situation and that of Fig. 12 is that the axial field profiles are always those of gyrotron oscillation. In the present experiment, the power supply sets a proper voltage rise time, and single-mode oscillation of the $TE_{22,2}$ mode is realized as shown in Fig. 11.

Many other modes exist between the $TE_{22,2}$ mode and the $TE_{21,2}$ mode. However, they do not oscillate because the coupling coefficients of these modes are much lower than those of the $TE_{22,2}$ mode and the $TE_{21,2}$ mode for the beam radius that is optimal for the $TE_{21,2}$ mode. Strong interaction between the $TE_{22,2}$ mode and the $TE_{21,2}$ mode is a particular feature of WGMs, and sideband mode competition or mode hopping from the $TE_{21,2}$ mode to the $TE_{22,2}$ mode takes place [37, 38].

Fig. 14 Axial field profiles of the $TE_{21,2}$ mode and the $TE_{22,2}$ mode at different instances corresponding to the time evolution shown in Fig. 13. The three panels represent three specific times: 2 ns, 30 ns and 60 ns, respectively. The detuning factors for the $TE_{21,2}$ mode and the $TE_{22,2}$ mode are 0.08 and 0.67, respectively. The constant radius section of the cavity is from 5 mm to 13 mm. Down taper and up taper are attached to the left hand side and the right hand side.

5. Summary

A high power sub-THz gyrotron was fabricated based on careful design considerations. The design concept is the same as that used in the prototype gyrotron with the $TE_{14,2}$ mode. The higher mode $TE_{22,2}$ was adopted to reduce the Ohmic loss on the cavity surface for the desired power of 300 kW. Stable single-mode oscillation has been confirmed with a very simple power supply. The oscillation power and frequency are very stable over the entire pulse duration up to 100 μs. This pulse width is limited by the power supply. No parasitic mode was observed during the turn-on and turn-off phases of each pulse. Time evolution of the $TE_{22,2}$ mode and possible competing modes were calculated taking into account a finite voltage rise time. The $TE_{22,2}$ mode pulls itself up to the highest power state from backward wave oscillation for the finite voltage rise time corresponding to the experiment. On the other hand, the calculation indicates that, if the beam voltage rises instantaneously, mode hopping from the $TE_{21,2}$ mode to the $TE_{22,2}$ mode takes place in the magnetic field region where the $TE_{22,2}$ mode attains the highest power.

Acknowledgments

[1] K.E. Kreischer and R.J. Temkin, Phys. Rev. Lett. **59**, 547 (1987).

[2] D.R. Whaley, M.Q. Tran, A. Alberti, T.M. Tran, T.M. Antonsen and C. Tran, Phys. Rev. Lett. **75**, 1304 (1995).

[3] G.S. Nusinovich, O.V. Sinitsyn, L. Velikovich, M. Yeddulla, T.M. Antonsen, Jr., A.N. Vlasov, S.R. Cauffman and K. Felch, IEEE Trans. Plasma Sci. **32**, 841 (2004).

[4] D.S. Tax, O.V. Sinitsyn, W.C. Guss, G.S. Nusinovich, M.A. Shapiro and R.J. Temkin, IEEE Trans. Plasma Sci. **41**, 862 (2013).

[5] M.K.A. Thumm, IEEE Trans. Plasma Sci. **42**, 590 (2014).

[6] M. Thumm, J. Franck, P.C. Kalaria, K.A. Avramidis, G. Gantenbein, S. Illy, I.G. Pagonakis, M. Schmid, C. Wu, J. Zhang and J. Jelonnek, Terahertz Sci. Tech. **8**, 85 (2015).

[7] H. Bindslev, S.K. Nielsen, L. Porte, J.A. Hoekzema, S.B. Korsholm, F. Meo, P.K. Michelsen, S. Michelsen, J.W. Oosterbeek, E.L. Tsakadze, E. Westerhof, P. Woskov and the TEXTOR team, Phys. Rev. Lett. **97**, 205005 (2006).

[8] M. Nishiura, S. Kubo, K. Tanaka, R. Seki, S. Ogasawara, T. Shimozuma, K. Okada, S. Kobayashi, T. Mutoh, K. Kawahata, T. Watari, LHD experiment group, T. Saito, Y. Tatematsu, S.B. Korsholm and M. Salewski, Nucl. Fusion **54**, 023006 (2014).

[9] J. Rasmussen, S.K. Nielsen, M. Stejner, J. Galdon-Quiroga, M. Garcia-Munoz, B. Geiger, A.S. Jacobsen, F. Jaulmes, S.B. Korsholm, N. Lazanyi, F. Leipold, F. Ryter, M. Salewski, M. Schubert, J. Stober, D. Wagner, the ASDEX Upgrade Team and the EUROFusion MST1 Team, Nucl. Fusion **56**, 112014 (2016).

[10] K. Tanaka, M. Nishiura, S. Kubo, T. Shimozuma and T. Saito, J. Instrumentation **10**, C12001 (2015).

[11] T. Saito, T. Notake, Y. Tatematsu, A. Fujii, S. Ogasawara, La Agusu, T. Idehara, S. Kubo, T. Shimozuma, K. Tanaka, M. Nishiura, K. Kawahata and V.N. Manuilov, J. Phys.: Conf. Series **227**, 012013 (2010).

[12] S. Ogasawara, S. Kubo, M. Nishiura, Y. Tatematsu, T. Saito, K. Tanaka, T. Shimozuma, Y. Yoshimura, H. Igami, H. Takahashi, S. Ito, Y. Takita, S. Kobayashi, Y. Mizuno, K. Okada, R. Minami, T. Kariya and T. Imai, Plasma Fusion Res. **7**, 2405061 (2012).

[13] T. Notake, T. Saito, Y. Tatematsu, A. Fujii, S. Ogasawara, La Agusu, I. Ogawa, T. Idehara and V.N. Manuilov, Phys. Rev. Lett. **103**, 225002 (2009).

[14] T. Saito, Y. Tatematsu, Y. Yamaguchi, S. Ikeuchi, S. Ogasawara, N. Yamada, R. Ikeda, I. Ogawa and T. Idehara, Phys. Rev. Lett. **109**, 155001 (2012).

[15] T. Saito, N. Yamada, S. Ikeuti, S. Ogasawara, Y. Tatematsu, R. Ikeda, I. Ogawa, T. Idehara, V.N. Manuilov, T. Shimozuma, S. Kubo, M. Nishiura, K. Tanaka and K. Kawahata, Phys. Plasmas **19**, 063106 (2012).

[16] K. Sakamoto, A. Kasugai, K. Kajiwara, K. Takahashi, Y. Oda, K. Hayashi and N. Kobayashi, Nucl. Fusion **49**, 095019 (2009).

[17] G.S. Nusinovich, A.N. Vlasov, T.M. Antonsen, Jr., J. Lohr, B.G. Danly and J.-H. Hogge, Phys. Plasmas **15**, 103101 (2008).

[18] K.E. Kreischer, T.L. Grimm, W.C. Guss, A.W. Mobius and R.J. Temkin, Phys. Fluids **B2**, 640 (1990).

[19] K. Felch, T.S. Chu, J. Feinstein, H. Huey, H. Jory, J. Neilsen and R. Schumacher, "Long-pulse operation of a gyrotron with beam/RF separation", Conf. Digest of 17th Int. Conf. Infrared Milli. Waves, 14 - 17 December 1992, Pasadena, USA, T4.1.

[20] K. Sakamoto, M. Tsuneoka, A. Kasugai, T. Imai, T. Kariya, K. Hayashi and Y. Mitsunaka, Phys. Rev. Lett. **73**, 3532 (1994).

[21] Y. Yamaguchi, T. Saito, Y. Tatematsu, S. Ikeuchi, V.N. Manuilov, J. Kasa, M. Kotera, T. Idehara, S. Kubo, T. Shimozuma, K. Tanaka and M. Nishiura, Nucl. Fusion **55**, 013002 (2015).

[22] Y. Tatematsu, Y. Yamaguchi, T. Idehara, T. Ozeki, R. Ikeda, T. Kanemaki, I. Ogawa and T. Saito, J. Infrared Milli. Terahz Waves **33**, 292 (2012).

[23] M.V. Kertikeyan, E. Borie and M.K.A. Thumm, *Gyrotrons* (Springer-Verlag, Berlin, 2004).

[24] Y. Yamaguchi, J. Kasa, T. Saito, Y. Tatematsu, M. Kotera, S. Kubo, T. Shimozuma, K. Tanaka and M. Nishiura, J. Instrumentation **10**, C10002 (2015).

[25] Y. Yamaguchi, Y. Tatematsu, T. Saito, R. Ikeda, J.C. Mudiganti, I. Ogawa and T. Idehara, Phys. Plasmas **19**, 113113 (2012).

[26] Y. Tatematsu, Y. Yamaguchi, T. Idehara, T. Kawase, I. Ogawa, T. Saito and T. Fujiwara, J. Infrared Milli. Terahz Waves **35**, 517 (2014).

[27] T. Saito, Y. Yamaguchi, M. Fukunari, Y. Tatematsu, T. Hirobe, R. Shinbayashi, S. Tanaka, S. Kubo, T. Shimozuma, K. Tanaka and M. Nishiura, "Design Consideration and Oscillation Characteristics of High-Power 300 GHz Gyrotron", IRMMW-THz 2017, Cancún, México, Aug. 27 - Sep. 1, 2017, RA2.1.

[28] T. Saito, S. Tanaka, R. Shinbayashi, T. Hirobe, Y.

Yamaguchi, M. Fukunari, Y. Tatematsu, K. Ohkubo, S. Kubo, T. Shimozuma, K. Tanaka and M. Nishiura, "Developments of Equipment for Sub-THz Collective Thomson Scattering in LHD", IRMMW-THz 2018, Nagoya, Japan, Sep. 9 - Sep. 14, 2018, Tu-P2-R1-2.

[29] T. Saito, Y. Yamaguchi, Y. Tatematsu, M. Fukunari, T. Hirobe, S. Tanaka, R. Shinbayashi, T. Shimozuma, S. Kubo, K. Tanaka and M. Nishiura, Plasma Fusion Res. **12**, 1206013 (2017).

[30] T. Hirobe, R. Shinbayashi, S. Tanaka, T. Yokoyama, Y. Yamaguchi, M. Fukunari, T. Saito, Y. Tatematsu, K. Ohkubo, S. Kubo, T. Shimozuma, K. Tanaka and M. Nishiura, "Transmission Test of 300 GHz Band Gyrotron Power for CTS Diagnostics by Corrugated Waveguides II", Plasma Conference 2017, Himeji, Japan, November 20 - 24, 2017, 21P-53.

[31] S. Ogasawara, S. Kubo, M. Nishiura, Y. Tatematsu, T. Saito, K. Tanaka, T. Shimozuma, Y. Yoshimura, H. Igami,

H. Takahashi, S. Ito, Y. Takita, S. Kobayashi, Y. Mizuno, K. Okada, R. Minami, T. Kariya and T. Imai, Rev. Sci. Instrum. **83**, 10D731 (2012).

[32] A. Schlaich, C. Wu, I. Pagonakis, K. Avramidis, S. Illy, G. Gantenbein, J. Jelonnek and M. Thumm, J. Infrared Milli. Terahz Waves **36**, 797 (2015).

[33] G.S. Nusinovich, M. Yeddulla, T.M. Antonsen and A.N. Vlasov, Phys. Rev. Lett. **96**, 125101 (2006).

[34] O. Dumbrajs, T. Saito and Y. Tatematsu, Phys. Plasmas **23**, 023106 (2016).

[35] B.G. Danly and R.J. Temkin, Phys. Fluids **29**, 561 (1986).

[36] G.S. Nusinovich, *Introduction to the Physics of Gyrotrons* (The Johns Hopkins University Press, Baltimore and London, 2004).

[37] W.C. Guss, M.A. Basten, K.E. Kreischer and R.J. Temkin, Phys. Rev. Lett. **69**, 3727 (1992).

[38] B. Levush and T.M. Antonsen, IEEE Trans. Plasma Sci. **18**, 260 (1990).